Electromagnetic Wave Propagation Through Chaff Clouds

Sherman W. Marcus, *Senior Member, IEEE*

***Abstract*—The computation of electromagnetic wave scattering by clouds of dipoles is straightforward when the dipole density is small. For higher density clouds, the coupling effects between the dipoles and their attenuation effects on the wave must be considered. This is accomplished herein by replacing the randomly distributed dipoles in the cloud by a conducting continuum. The conductivity of this continuum is determined by requiring that the radar cross section (RCS) of an infinitesimally thin slab of the continuum be the same as that of a similar portion of the dipole cloud. The thinness of this reference dipole cloud eliminates the necessity to consider inter-dipole coupling. The reflection and transmission characteristics of the cloud are then obtained using standard methods for propagation through the effective conductor. RCS results are shown to agree with coupled numerical integral equation solutions for scattering from a closely spaced system of wires. Simple formulas are derived for the attenuation effects of the dipole cloud. For most cases of interest, the wave with wave length λ attenuates through a cloud of half wave dipoles of density ρ at the rate of $0.655(\rho\lambda^3)$ dB per λ.**

***Index Terms*—Electromagnetic propagation, electromagnetic scattering by random media, radar cross section (RCS).**

I. Introduction

THE scattering by clouds of wire dipoles, or chaff, has been the subject of research for many decades. The main impetus for this research derived from its military applications for electromagnetic countermeasures to radar detection [1]. Nevertheless, in recent years chaff has also found civilian applications which take advantage of its ability to be detected by radar while remaining suspended for extended periods of time in the atmosphere [2], [3]. These include the study of atmospheric air flow and implementation of changes in atmospheric properties [4]–[7].

In most applications of chaff, the main interest is its backscatter of electromagnetic waves to the radar which transmitted them. This backscatter is characterized by the radar cross section (RCS) of the chaff cloud. For a cloud with dimensions that are large relative to the wave length λ of the incident radiation, and consisting of a dipole density ρ such that the dipoles are randomly separated from each other by distances large relative to λ, it has been shown that the RCS of many dipoles is the sum of the RCS of the individual dipoles [8], [9]. Since methods to compute the RCS of individual dipoles are readily available [10], [11], the determination of the backscatter effects of a large sparse cloud is straightforward in most instances if the statistical distributions of the dipole characteristics are known [3]. On the other hand, there are instances when a chaff cloud can be quite dense, usually shortly after dispersal. There are then two main effects which must be accounted for: Inter-dipole coupling which is a local effect, and shielding which is a global effect.

1) Inter-dipole coupling. When dipoles are sufficiently close together, the current induced in each one by the incident wave is affected by the currents induced in neighboring dipoles. This may be illustrated by a simple example of two parallel dipoles equidistant from the incident source of radiation (to assure the same phase). When the dipoles are far from each other, the current I induced in each would be approximately that which would be produced if the other wire were not present. As the two wires approach each other to become adjacent, their behavior approaches that of a single wire with *total* induced current I, so that the current induced in each will be $I/2$.
2) Shielding. If the dipole density is sufficiently large, the part of the cloud closest to the incident radiation source will shield the distant regions of the cloud so that less incident energy will reach them. Clearly, the dipoles in these distant regions re-radiate less energy and therefore will not contribute to the RCS in the same manner as the regions closer to the incident energy source. The shielding phenomenon is therefore dependent on the depth of penetration within the cloud as well as on the dipole density. Of course, in the extreme case in which the dipole density becomes infinite, the "cloud" would become a near perfect conductor and the electromagnetic fields would vanish beyond the region closest to the energy source.

The local effect, that of inter-dipole coupling, can be accounted for relatively simply by applying readily available numerical techniques to dipoles in a localized region [12]. These techniques divide the dipoles into elements over which the induced currents are solved by satisfying the boundary conditions along the wire surface. Such a technique has been used to compute the RCS for a small cloud of dipoles as a function of its average dipole spacing [8]. This *coupled* RCS for each dipole could then be used in place of the uncoupled RCS in cloud calculations as long as the effect of shielding can be neglected.

Determination of the shielding is somewhat more difficult since, as a global effect, it is influenced by many more dipoles. A full solution of the coupled equations for this problem is therefore impractical so that other methods must be sought. One such method which has been proposed is based on energy "removed" from the propagation direction [9], [13], and models the cloud as a slab on which the energy is normally incident, say in the

Manuscript received October 11, 2005; revised December 20, 2006.

The author is with RAFAEL, Haifa 31021, Israel (e-mail: shermanm@ieee.org).

Color versions of one or more of the figures in this paper are available online at http://ieeexplore.ieee.org.

Digital Object Identifier 10.1109/TAP.2007.900178

x-direction. Following [13], the power flow dS removed from a strip dx of the slab is given by

$$dS = -\frac{1}{2}\langle\sigma_s\rangle S(x)\rho dx \tag{1}$$

where $S(x)$ is the power flow (Poynting vector) magnitude at the depth x within the slab, and $\langle\sigma_s\rangle$ is the total scattering cross section of a dipole averaged over all of its possible orientations. Equation (1) is integrated over the width of the slab to obtain the total energy attenuation throughout the slab. This result was found to require revision when the slab width is small [13]. The basis of this inconsistency will now be discussed.

The energy flow formulation as characterized by (1) is fraught with difficulties. The most blatant of these is the implication in (1) that the total cross section of the dipoles within the strip dx is the *sum* of the average cross section $\langle\sigma_s\rangle$ of each of the dipoles. As indicated above, this has been shown to be true for dipoles randomly distributed over a large volume, but only when this volume spans a region that is large in the direction of propagation x; only then would the phase of each dipole contribution be random and the summation of $\langle\sigma_s\rangle$ be justified. The volume considered in (1), however, only extends over the differential distance dx in the direction of propagation, so that the phases of the induced currents in all the dipoles of that differential volume are similar. The average cross sections therefore cannot be summed. A corollary to this is that (1) implies that the power flow removed from a differential volume is proportional to dx whereas in fact it is proportional to dx^2 (see Section III). Finally, since (1) is devoid of phase information, it cannot account for interference effects caused by the slab boundaries or by reflections from targets beyond the chaff cloud.

In what follows, a new approach is described for determining the effects of electromagnetic wave propagation through a chaff cloud, and the resulting shielding effect of the cloud. The approach is implemented in the realm of induced currents which combine vectorially, thereby avoiding the pitfalls of energy additions. The outputs, however, are of course provided in terms of power flow and are related to RCS. In order to maintain compatibility with [9] and [13], and for purposes of tractability, the cloud will be modeled as a slab containing randomly oriented dipoles. In Section II, the problem is formulated and the current induced in dipoles in a narrow layer of the cloud is approximated as a current density. With the help of Ohm's Law, it is shown that the slab of discrete dipoles can be considered as a homogenous slab with an effective conductivity. This reduces the problem to one of propagation through a layered medium as described in Section III in which expressions for the reflection and transmission coefficients are defined and related to RCS. The behavior of these coefficients as a function of cloud thickness is presented in Section IV. Also presented in Section IV are comparisons between the RCS of an effective conductor and the numerically determined RCS of a cloud of dipoles.

II. Equivalent Conductor Hypothesis

Consider a cloud of randomly oriented dipoles the centers of which are randomly distributed throughout a slab which extends from $x = 0$ to $x = d$ (region 1 in Fig. 1). The dipoles are

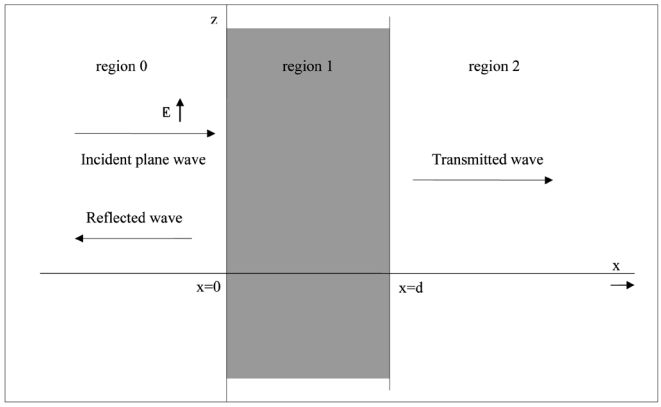

Fig. 1. A dipole cloud slab.

randomly oriented so that the wire direction $\hat{\ell}$ is uniformly distributed over all solid angles. A plane wave propagating in the $\hat{\mathbf{x}}$ direction and characterized by an angular velocity ω is incident on the slab from the free space $\mathrm{x} < 0$ (region 0), where $\omega = 2\pi f$ and f is the frequency. The wave number in region i of the figure is given by

$$k_i = \omega\sqrt{\mu_i\varepsilon_i} \tag{2}$$

where ε_i and $\mu_i = \mu_0$ are the values of permittivity and permeability in the respective medium. The electric field of the incident wave is $\mathbf{E}_{\mathrm{inc}} = E_{\mathrm{inc}}e^{-jk_0x}\hat{\mathbf{z}}$, where an $e^{j\omega t}$ time dependence has been assumed. This wave induces currents in the dipoles so that the boundary conditions will be satisfied along the wires.

It is clear that in the limit in which the dipole density ρ is such that the wires are closely packed, the boundary conditions which must be satisfied at $x = 0$ will be those between free space and the wire material. That is, the cloud in this limit will become a continuous conductor. The field within this conductor will be given by

$$\mathbf{E}_1 = \mathbf{E}_{\mathrm{inc}} + E_{\mathrm{scat}}(x)\hat{\mathbf{z}} \tag{3}$$

where E_{scat} is the field caused by the presence of the conductor. The total field $\mathbf{E}_1$ will attenuate as the penetration depth x increases as will the induced current density $\mathbf{J}$ in accordance with Ohm's law

$$\mathbf{J}(x) = \sigma_1\mathbf{E}_1(x), 0\langle x\langle d \tag{4}$$

where σ_1 is the conductivity in the dipole region. If σ_1 is not infinite, then as $d \to 0, E_{\mathrm{scat}}(x) \to 0$ and $\mathbf{J}(0) \to \sigma_1 E_{\mathrm{inc}}\hat{\mathbf{z}}$. Alternatively, if $\mathbf{J}(0)$ were known as $d \to 0$, then the conductivity could be found from

$$\sigma_1 = \frac{J(0)}{E_{\mathrm{inc}}}. \tag{5}$$

It should be noted that in the limit considered, E_{scat}, which is produced by $J(0)$, *approaches* 0, but is not actually zero unless $d = 0$. It is, however, small relative to E_{inc} and can therefore be ignored in (5). However, E_{scat} or equivalently $J(0)$ can be used to determine the radiation contributions far from the slab. It should also be noted that if d were now increased to a large

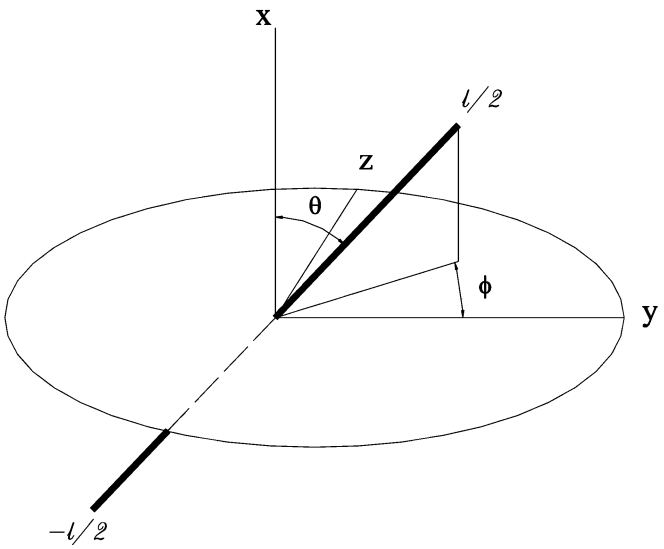

Fig. 2. Coordinate system for a single dipole.

value, the conductivity found in (5) will still of course characterize the medium everywhere in region 1 even though it was found for the specific case of $d \to 0$.

The above was derived for the case of closely packed dipoles for which the cloud can be considered a continuum. Analogous derivations will now be sought for sparser dipole densities that are based on an *effective* uniform current density $J(0)$ over the volume of interest. This effective current density will be found by imposing the condition that the fields produced by it far from the dipole cloud be the same as the fields caused by the currents induced in the discrete random dipoles. The volume V of interest will be a cylindrical section of a narrow cloud of very small thickness d. If the radius of the cylindrical section is r_0, then the volume of the section is $\pi r_0^2 d$, and the axis of the cylinder corresponds to the x-axis. The vector potential $\mathbf{A}$, from which all field and energy flow quantities may be obtained, will be determined in the region $x \to -\infty, y = 0, z = 0$. For the z-directed uniform current density $J(0)$ within this disk, it is shown in (B6) of the Appendix that

$$\mathbf{A}(\mathbf{r}) \approx \frac{\mu_0 J(0) V e^{-jkx}\hat{\mathbf{z}}}{4\pi x}, J(0) \text{ uniform over } V. \tag{6}$$

Consider now the case of M discrete dipoles with particle density $\rho = M/(\pi r_0^2 d)$, and with an average inter-particle separation distance $r_{\text{sep}} \gg d$. Since $\pi r_0^2/M \sim r_{\text{sep}}^2$, it follows that $r_{\text{sep}} \sim (\rho d)^{-1/2}$. Therefore, for any given ρ the value of d can be made sufficiently small so that r_{sep} would be large enough to ignore the inter-dipole coupling. In addition, as a result of this thinness and as a result of the plane wave impinging normally on the slab, the phase of the incident wave at the center of each dipole will be approximately the same. Therefore, in the observation region of interest far from the slab, the locations of the dipoles are not significant, whereas their orientations are significant. Consider the typical dipole shown in Fig. 2 where the correspondence of the spherical coordinates to the Cartesian coordinates is not standard, but rather defined such that θ is measured relative to the direction of the incident wave vector. The dipole can be characterized by a vector $\vec{\ell}$ with magnitude equal to the length of the dipole, and with direction from the wire end at which x is minimum to the wire end at which x is maximum. The vector potential for this dipole is [14]

$$\mathbf{A}(\mathbf{r}) = \frac{\mu_0}{4\pi}\hat{\ell}\int_{-\ell/2}^{\ell/2} I(\ell')\frac{e^{-jk_0 R}}{R}d\ell' \tag{7}$$

where $R = \sqrt{r^2 + \ell'^2 - 2\ell' r(\hat{\mathbf{r}}\cdot\hat{\ell})} \approx r[1 - (\ell'/r)(\hat{\mathbf{r}}\cdot\hat{\ell})]$, and $\mathbf{r} = x\hat{\mathbf{x}} + y\hat{\mathbf{y}} + z\hat{\mathbf{z}}$ is the vector from the center of the dipole to the observation point. Therefore

$$\mathbf{A}(\mathbf{r}) = \frac{\mu_0 e^{-jk_0 r}}{4\pi r}\hat{\ell}\int_{-\ell/2}^{\ell/2} I(\ell')e^{jk_0\ell'(\hat{\mathbf{x}}\cdot\hat{\ell})}d\ell' \tag{8}$$

where $\hat{\mathbf{r}}$ has been replaced by $-\hat{\mathbf{x}}$ under the assumption that the point $\mathbf{r}$ is in the vicinity of $x \to -\infty, |y/x| \ll 1, |z/x| \ll 1$. Expressing the wire direction in spherical coordinates

$$\hat{\ell}(\theta,\phi) = \cos\theta\hat{\mathbf{x}} + \sin\theta\cos\phi\hat{\mathbf{y}} + \sin\theta\sin\phi\hat{\mathbf{z}} \tag{9}$$

where θ is the angle of the wire with the positive x-axis and ϕ is the angle of the projection of the wire direction onto the y-z plane relative to the y-axis positive counter-clockwise. Equation (8) can therefore be written

$$\begin{aligned}\mathbf{A}(\mathbf{r};\theta,\phi) &= \frac{\mu_0 e^{-jk_0 r}}{4\pi r}\hat{\ell}(\theta,\phi)\int_{-\ell/2}^{\ell/2} I(\ell';\theta,\phi)e^{jk_0\ell'\cos\theta}d\ell' \\ &= \frac{\mu_0 e^{-jk_0 r}\ell\lambda}{4\pi r}\tilde{\mathbf{I}}(\theta,\phi)\end{aligned} \tag{10}$$

where

$$\tilde{\mathbf{I}}(\theta,\phi) = \frac{\hat{\ell}(\theta,\phi)}{\ell}\int_{-(\ell/\lambda)/2}^{(\ell/\lambda)/2}[I(\ell';\theta,\phi)e^{j2\pi(\ell'/\lambda)\cos\theta}d(\ell'/\lambda) \tag{11}$$

is the average of each vector component of $\hat{\ell}(\theta,\phi)I(\ell';\theta,\phi)e^{jk_0\ell'\cos\theta}$ per unit wave length over the length of the wire, and the integral in (11) has been normalized.

Consider now the vector potential of all M dipoles within a volume V of the thin slab, where the linear dimensions of V are much less than r. Since the dipole orientations are random, all orientations are present in principle. The total vector potential at $\mathbf{r}$ due to all the dipoles will then be given by the product of M and the average vector potential over all orientations

$$\mathbf{A}_{\text{total}}(\mathbf{r}) = \frac{\mu_0 e^{-jk_0 r}\ell\lambda}{4\pi r}M\bar{\mathbf{I}} \tag{12}$$

where

$$\bar{\mathbf{I}} = \frac{1}{4\pi}\int_0^{\pi} d\theta\sin\theta\int_0^{2\pi} d\phi\tilde{\mathbf{I}}(\theta,\phi) \tag{13}$$

is the average value of $\tilde{\mathbf{I}}(\theta,\phi)$ over all orientations. It will be noticed from (11) that if the dipole orientations were constrained to be parallel to the y-z plane (i.e., $\theta = 90°$), then the phase in the exponential term would vanish and $\bar{\mathbf{I}}$ would represent the average of the actual current components.

The components of $\bar{\mathbf{I}}$ will now be considered under the continued assumption that the dipoles are sufficiently far apart from each other that there is no coupling between them, and that their centers lie in the same y- z plane. In such a case, only the component of the polarization vector in the plane of incidence formed by the wire and the wave vector contributes to the induced current. This component is $\mathbf{t} = \hat{\mathbf{z}} - (\hat{\mathbf{z}}\cdot\hat{\mathbf{n}})\hat{\mathbf{n}}$ where $\hat{\mathbf{n}} = -\sin\phi\hat{\mathbf{y}} + \cos\phi\hat{\mathbf{z}}$ is the unit vector perpendicular to the incidence plane. Since $|\mathbf{t}| = |\sin\phi|$, the functional dependence of the current may be written

$$I(\ell';\theta,\phi) = I(\ell';\theta)\sin\phi \tag{14}$$

where $I(\ell';\theta) = I(\ell';\theta,\phi=\pi/2)$. From (9), (11), (13), and (14), the x- and y-components of $\bar{\mathbf{I}}$ are

$$\bar{\mathbf{I}}\cdot\hat{\mathbf{x}} = \frac{1}{4\pi\ell}\int_0^{\pi} d\theta\sin\theta\cos\theta \times \int_{-(\ell/\lambda)/2}^{(\ell/\lambda)/2}[I(\ell';\theta)e^{j2\pi(\ell'/\lambda)\cos\theta}d(\ell'/\lambda) \times \int_0^{2\pi} d\phi\sin\phi \tag{15a}$$

$$\bar{\mathbf{I}}\cdot\hat{\mathbf{y}} = \frac{1}{4\pi\ell}\int_0^{\pi} d\theta\sin^2\theta \times \int_{-(\ell/\lambda)/2}^{(\ell/\lambda)/2}[I(\ell';\theta)e^{j2\pi(\ell'/\lambda)\cos\theta}d(\ell'/\lambda) \times \int_0^{2\pi} d\phi\cos\phi\sin\phi. \tag{15b}$$

In both these equations, the last integral vanishes, so that the surviving z-component of (13) may be written

$$\bar{\mathbf{I}} = \frac{\hat{\mathbf{z}}}{4\pi\ell}\int_0^{\pi} d\theta\sin^2\theta\int_0^{2\pi} d\phi\sin^2\phi \times \int_{-(\ell/\lambda)/2}^{(\ell/\lambda)/2}[I(\ell';\theta)e^{j2\pi(\ell'/\lambda)\cos\theta}d(\ell'/\lambda) = \frac{\hat{\mathbf{z}}}{4\ell}\int_0^{\pi} d\theta\sin^2\theta \times \int_{-(\ell/\lambda)/2}^{(\ell/\lambda)/2}[I(\ell';\theta)e^{j2\pi(\ell'/\lambda)\cos\theta}d(\ell'/\lambda). \tag{16}$$

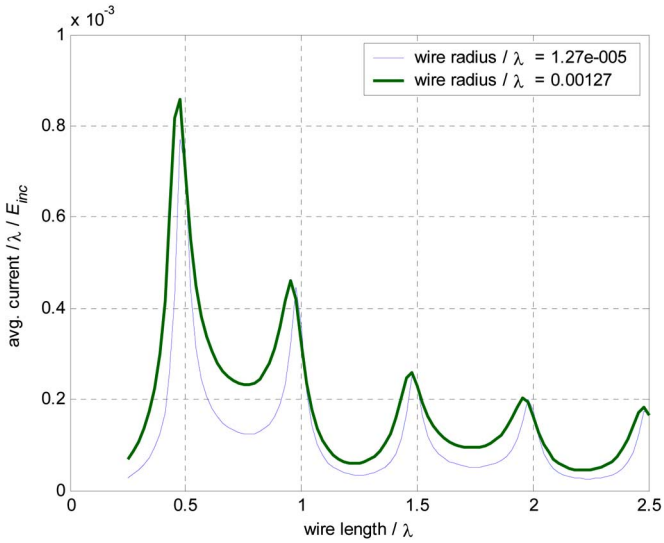

Fig. 3. $\bar{I}$ as a function of ℓ/λ for two values of dipole radius.

Numerically computed results for $\bar{I}$ are shown in Fig. 3 as a function of ℓ/λ for two values of wire radius [12].

From (12) and (16)

$$\mathbf{A}_{\text{total}}(\mathbf{r}) = \frac{\mu_0 e^{-jk_0 r}\ell\lambda}{4\pi r}M\bar{I}\hat{\mathbf{z}}. \tag{17}$$

Since $\mathbf{A}_{\text{total}}$ has only a $\hat{\mathbf{z}}$ component, and since in (12) $r \to -x \to \infty$, the procedure used in (B6) to (B9) can be employed to show that at $\mathbf{r}$—for scattering from the slab of randomly oriented dipoles—the average scattered E-field is in the $\hat{\mathbf{z}}$ direction and the average power flow is in the $-\hat{\mathbf{x}}$ direction. This is known to be the case for coherent scattering from a slab of random scatterers [15, Ch. 14].

Comparing (17) with (6), it is seen that for an observation point far from the slab, the vector potential for a uniform current density within the continuum volume V would be identical to the vector potential for discrete randomly oriented dipoles within that volume if the current density satisfied

$$\mathbf{J}(0) = \frac{\hat{\mathbf{z}}M\ell\lambda\bar{I}E_{\text{inc}}}{V} = \hat{\mathbf{z}}\rho\ell\lambda\bar{I}E_{\text{inc}} \tag{18}$$

which is seen to be explicitly independent of the size or shape of the region V. This current density may now be used in (5) to obtain the effective conductivity σ_1 of the medium which, as required, is not dependent on E_{inc}. It is more convenient though to use the non-dimensional parameter s defined in (C2). When using (5) and (18), this may be written

$$s = \frac{\sigma_1}{\varepsilon_0\omega} = c_1(\rho\lambda^3)\frac{\ell}{\lambda}\bar{I} \tag{19}$$

where $c_1 = (\eta_0/2\pi) \approx 60$ ohms when $\bar{I}$ is expressed in 1/ohms, and

$$\eta_i = \frac{\omega\mu_i}{k_i} = \sqrt{\frac{\mu_i}{\varepsilon_i}} \tag{20}$$

is the impedance of medium i. Since $\bar{I}$ in Fig. 3 does not exceed 10^{-3}, $s < 0.06(\rho\lambda^3)(\ell/\lambda)$.

The far field equivalence between a dipole cloud and a conducting continuum was proved here for a narrow cloud. It would be hoped that a wide conducting continuum would similarly provide far fields that are representative of a correspondingly wide dipole cloud. Inter-dipole coupling would actively be accounted for in such a wide cloud by the interaction between each "narrow" cloud of which it is composed. Thus, if two narrow conducting slabs of width $d/2$ are placed adjacent to each other to form a single conducting slab of width d, it is clear that the presence of each half-slab will influence the field in the other. It is this coupling effect which is meant to model the corresponding coupling in a slab of discrete dipoles. However, even for a defined average density ρ, the magnitude and direction of $\mathbf{E}$ in the far field of the dipole cloud can also be expected to fluctuate with changes in the specific locations and orientations of its component dipoles, and can thereby produce power flow in directions other than the $-\hat{\mathbf{x}}$ direction. In Section IV, such fluctuations will be associated with an "incoherent" contribution to the RCS, while the conducting continuum will be shown to be compatible with the "coherent" contribution.

The simulation of the discrete dipole cloud by a conducting continuum will be used in the following section to obtain reflection and transmission coefficients for propagation through the cloud when modeled as an equivalent conducting continuum.

III. Propagation Through the Equivalent Conducting Slab

1) Governing Equations: In each medium i of Fig. 1 the z-directed electric field satisfies the Helmholtz equation

$$\nabla^2 E_i + k_i^2 E_i = 0, \quad 0 \leqslant i \leqslant 2 \tag{21}$$

the solutions of which are

$$E_i(x) = A_i e^{-jk_i x} + B_i e^{jk_i x} \tag{22}$$

where the k_i were defined in (2), and the terms on the right represent waves traveling in the positive and negative x-directions. In region 0, the wave in the positive x-direction is the incident wave, so that $A_0 = E_{\text{inc}}$ which will be assumed to be unity. In region 2, there is no incoming wave so $B_2 \equiv 0$. From the relation

$$-j\omega\mu_i \mathbf{H}_i = \nabla \times \mathbf{E}_i = -\hat{\mathbf{y}} \frac{\partial E_i}{\partial x} \tag{23}$$

the y-directed magnetic field in each medium is

$$H_i(x) = -A_i \frac{1}{\eta_i} e^{-jk_i x} + B_i \frac{1}{\eta_i} e^{jk_i x} \tag{24}$$

where the η_i were defined in (20).

2) Solutions of Equations: The unknown coefficients B_0, A_1, B_1, A_2 may be determined from the four equations expressing the continuity of the tangential components of $\mathbf{E}$ and $\mathbf{H}$ at the two boundaries of the slab. This results in

$$B_0(s, d/\lambda) = \frac{2j(1-\beta^2)\sin\alpha}{(1+\beta)^2 e^{j\alpha} - (1-\beta)^2 e^{-j\alpha}} \quad \text{region 2 free space} \tag{25}$$

$$A_2(s, d/\lambda) = \frac{4\beta e^{j2\pi(d/\lambda)}}{(1+\beta)^2 e^{j\alpha} - (1-\beta)^2 e^{-j\alpha}} \quad \text{region 2 freespace} \tag{26}$$

where

$$\alpha \equiv k_1 d = 2\pi\beta(d/\lambda) \quad \beta \equiv \frac{\eta_0}{\eta_1}. \tag{27}$$

In Appendix C it is shown that β is a function only of s, so that the functional dependence of both B_0 and A_2 is only on the two parameters s and d/λ.

The solutions (25) and (26) were obtained for the case in which region 2 is free space. It is of interest to also consider the case in which region 2 is a perfect conductor which can simulate the presence of an idealized target beyond the chaff cloud. In such a situation,

$$B_0(s, d/\lambda) = \frac{(1-\beta)e^{j\alpha} - (1+\beta)e^{-j\alpha}}{(1+\beta)e^{j\alpha} - (1-\beta)e^{-j\alpha}} \quad \text{region 2 perfect conductor.} \tag{28}$$

3) Transmission and Reflection Coefficients: The average real power flow in each medium i is given by [14]

$$\mathbf{S}_i = \frac{1}{2}\text{Re}(\mathbf{E}_i \times \mathbf{H}_i^*) \tag{29}$$

where $*$ indicates complex conjugate. From (22) and (24), and confining consideration to free space for which the wave number and impedance are real

$$\begin{aligned}\mathbf{S}_i &= \frac{\hat{\mathbf{x}}}{2\eta_0}\text{Re}[|A_i|^2 - |B_i|^2 + (B_i A_i^*)e^{2jk_0 x} \\ &\quad - (B_i^* A_i)e^{-2jk_0 x}] \\ &= \frac{\hat{\mathbf{x}}}{2\eta_0}\text{Re}\{|A_i|^2 - |B_i|^2 + 2j[\text{Re}(B_i A_i^*)\sin(2k_0 x) \\ &\quad + \text{Im}(B_i A_i^*)\cos(2k_0 x)]\}\end{aligned}$$

or

$$\mathbf{S}_i = \frac{\hat{\mathbf{x}}}{2\eta_0}(|A_i|^2 - |B_i|^2) \tag{30}$$

which is compatible with the interpretation that the coefficients A_i and B_i are associated with the waves in the positive and negative x-directions, respectively. In region 0, $A_0 = 1$ so that

$$\mathbf{S}_0 = \frac{\hat{\mathbf{x}}}{2\eta_0}(1 - |B_0|^2). \tag{31}$$

It is clear that the first term in parenthesis represents the power flow of the incident wave, and the second represents the power flow of the reflected wave. In region 2, $B_2 = 0$, so that

$$\mathbf{S}_2 = \frac{\hat{\mathbf{x}}}{2\eta_0}|A_2|^2 \tag{32}$$

represents the power flow of the transmitted wave if region 2 is free space. Since $|B_0|^2$ and $|A_2|^2$ represent the energy of the reflected and transmitted waves relative to the unit incident energy, these quantities represent the reflection and transmission coefficients for propagation through the effective conductor.

Since solutions are provided in the Appendix for several cases involving narrow slabs, it is of interest to obtain the reflection coefficient from the Taylor expansion of (25) about $d = 0$. Using (C11)

$$|B_0|^2 = \frac{|1-\beta^2|^2}{4}(k_0 d)^2 + O[(k_0 d)^3] \approx \left(\frac{sk_0 d}{2}\right)^2, d \ll 1 \quad (33)$$

where s is given in (19). The average real power flow in the reflected direction is therefore

$$\mathbf{S}_{\text{refl}} = -\frac{\hat{\mathbf{x}}}{2\eta_0}\left(\frac{sk_0 d}{2}\right)^2. \quad (34)$$

On the other hand, the average real power flow radiated from the induced current density $J(0)$ in the same slab is derived in (A6) as

$$\mathbf{S}_{\text{avg}} = -\eta_0 |J(0)|^2 \frac{d^2}{8}\hat{\mathbf{x}}. \quad (35)$$

Using (5), (20) and (C2), this result is seen to be identical to (34), thereby demonstrating the consistency of the two methods.

4) Radar Cross Section: The concept of radar cross section generally refers to a localized object or target. When dealing with an object of infinite extent such as a slab, this concept must be revised slightly so that instead of referring to the RCS of the entire scattering body, it refers to a particular section of it. That is, for the slab of infinite extent, reference will be made to the RCS per unit area of the slab, where the unit area lies in the y-z plane.

The face $x = 0$ of the conducting slab continuum is a plane and all energy effectively flows normal to it. Assume for the moment that the slab is perfectly conducting. It is known that the RCS from a portion of such a plane of area A is given by [16]

$$\text{RCS} = \frac{4\pi}{\lambda^2}A^2 = \frac{k_0^2}{\pi}A^2, \text{conducting plate.} \quad (36)$$

But since the plate is perfectly conducting, (36) represents the case when all the energy that is incident is scattered back, which is tantamount to a reflection coefficient $|B_0|^2 = 1$. For any other value of $|\text{B}_0|^2$ the RCS due to an area A of the slab will be reduced accordingly. Therefore, for a non-perfectly-conducting slab, the RCS due to an area A of the slab will be given by

$$\text{RCS} = \frac{k_0^2 A^2}{\pi}|B_0|^2, \text{general slab.} \quad (37)$$

To confirm the consistency of this formula, consider the case of the unit field incident normally on a narrow slab of width d with effective conductivity σ. The reflection coefficient for this case was given in (33). On the other hand, consider the current density induced in the disk of area A of the same slab, as considered in Appendix B. The electric field due to this current density at $x \to \infty$ is given in (B7). From Ohm's law, the same scattered E-field will be obtained if the current density is replaced by a conductor with conductivity $\sigma = J_0/E_{\text{inc}}$ that is illuminated by an incident field E_{inc} polarized in the z-direction

$$\mathbf{E} = -\frac{jk_0^2 V}{4\pi x}s\mathbf{E}_{\text{inc}}e^{-jk_0 x} \quad (38)$$

where (C2) was used. The RCS is then given by [17]

$$\text{RCS} \underset{\lim x\to\infty}{=} 4\pi x^2 \frac{\mathbf{E}\cdot\mathbf{E}^*}{\mathbf{E}_{\text{inc}}\cdot\mathbf{E}_{\text{inc}}^*} = \frac{1}{4\pi}\left(k_0^2 sV\right)^2 \text{ disk of area } A. \quad (39)$$

It is clear that this RCS obtained for a disk of radius A and based on the vector potential derivation in Appendix B is identical to the RCS obtained from (37) and (33) for the same disk portion of an infinite slab, and obtained from the solution of the layered medium of Fig. 1.

The normalized backscatter RCS per unit area of the conducting slab can be obtained from (37) as

$$\nu_{\text{back}} = \frac{\text{RCS}/A}{(A/\lambda^2)} = \frac{\text{RCS}}{(A^2/\lambda^2)} = 4\pi|B_0|^2. \quad (40)$$

For forward scatter, the transmission coefficient A_2 cannot be used in analogy to B_0 in (40) since A_2 characterizes the total power flow consisting of both the incident and scattered waves, while the RCS characterizes the scattered wave alone. Since the total amplitude is given by (22), the amplitude of the scattered wave in region 2 is $(A_2 - 1)e^{-jk_0 x}$ so that the normalized forward scatter RCS per unit area is

$$\nu_{\text{forward}} = \frac{\text{RCS}}{(A^2/\lambda^2)} = 4\pi|A_2 - 1|^2. \quad (41)$$

IV. Results and Discussion

In Section II the following was shown.

1) a chaff cloud and a continuous conducting medium have the same qualitative effect on an electromagnetic wave passing through it;
2) a closely packed chaff cloud is *identical* to a continuous conductor;
3) a general chaff cloud of very small thickness will exhibit the same far field scattering effects as a continuous conductor with the same thickness and with conductivity that depends on the cloud characteristics.

In Section III the equations for propagation through a continuous conductor with material parameters based on item (3) above were developed and related to the far field parameter RCS. In this section, further evidence will be presented to corroborate the validity of the "equivalent conductor" hypothesis, and results and simplified expressions will be presented using the equations of Section III.

1) Cloud-Conductor Comparison: It is quite impossible to numerically calculate the coupling effects between dipoles spread over a large portion of a slab. However, in the comparison made between (34) and (35), it was shown that the scattering per area due to the currents in the entire slab is the same as if only the currents in that area were present. Therefore, in order to test (40), direct scattering computations were performed on a dipole cloud that is localized within a circular area A of the slab with non-negligible thickness d relative to λ, where the area A lies in the y-z plane and the thickness d is measured along the x-direction. A given number N of randomly oriented half-wave dipoles were randomly distributed throughout this cylindrically shaped volume V. Since the dipole density ρ and the slab width d are given, the

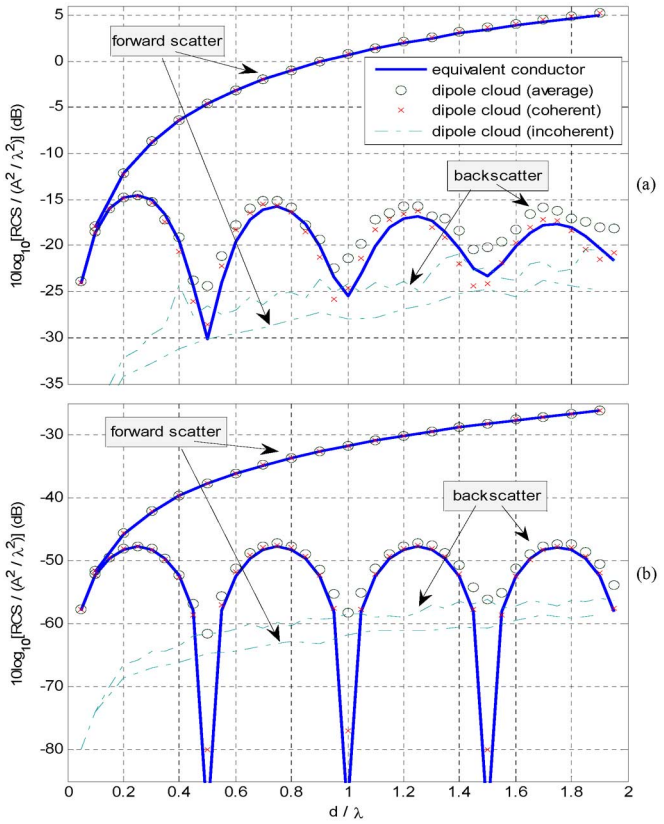

Fig. 4. Comparison of the backscatter RCS from a discrete cloud of half wave dipoles and an equivalent conducting continuum for (a) $\rho = 5/\lambda^3 (s = 0.116)$, (b) $\rho = 0.1/\lambda^3 (s = 0.0023)$.

fact that N is given in this numerical experiment implies that the volume and the area of the cylinder will be

$$V = N/\rho, \quad A = V/d. \tag{42}$$

The above data was used in the method-of-moments NEC program to numerically determine the RCS of the dipole "cloud" from the scattered z-component of the E-field [12]. The computations were performed using $N = 196$ for $d/\lambda \leqslant 0.2$, while for larger values of d/λ the value of N was chosen in accordance with (42) to maintain the same dipole density over the same cross sectional area as that used for $d/\lambda = 0.2$. Each dipole was divided into 3 segments, so that for $d/\lambda \leqslant 0.2$, a linear system of 588 equations was solved, while for $d/\lambda = 2.0$, the linear system consisted of about 6000 equations. Fifty different calculations were performed for each value of d/λ.

Fig. 4 displays backscatter and forward scatter RCS results for both the discrete dipole cloud and the equivalent conductor (EC) as a function of d/λ. The RCS results for the discrete dipole cloud include the average $\bar{\nu}$ of the $M = 50$ calculations, and the coherent and incoherent components $\nu_{\text{coh}}, \nu_{\text{incoh}}$ of this average (see Appendix D). In Fig. 4(a), a relatively high density $\rho = 5/\lambda^3 (s = 0.116)$ was used, while in Fig. 4(b) a relatively low dipole density $\rho = 0.1/\lambda^3 (s = 0.0023)$ was considered. Since the scattering by each dipole is azimuthally uniform, the backscattering and forward scattering RCS of the cloud are identical for small values of d/λ. For larger values of d/λ, the forward scattered fields due to dipoles at each depth of the slab have approximately the same phase so that this RCS increases with d/λ.

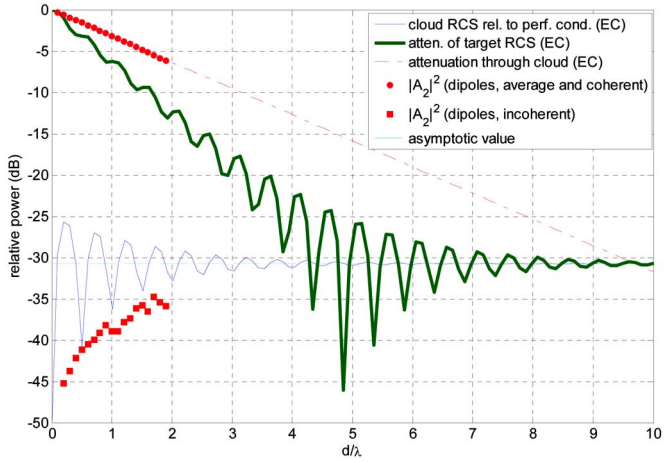

Fig. 5. Transmission and reflection coefficients for propagation through a dipole cloud, $\rho = 5/\lambda^3 (s = 0.116)$.

The phase of the corresponding backscattered fields, however, are different resulting in the oscillatory dependence of RCS on d/λ. This oscillatory behavior that is predicted by the EC method cannot be predicted by the energy flow method of (1).

For the two dipole densities considered in Fig. 4, it may be seen that (a) the $\bar{\nu}$ dipole cloud results and the EC method results are almost indistinguishable for forward scatter, (b) $\nu_{\text{incoh}} \rangle \nu_{\text{coh}}$ only at or near the backscatter nulls at $d/\lambda = n/2, n \geqslant 1$, and (c) good agreement is observed between ν_{coh} and EC for both forward and backscatter. From observations (b) and (c), and since the nulls in Fig. 4(b) are very deep, $\nu_{\text{incoh}} \ll \nu_{\text{coh}}$ near the backscatter peaks so that the EC results agree well with $\bar{\nu}$ for this low dipole density case. On the other hand, since the nulls of Fig. 4(a) are not deep and in fact become less deep as d/λ increases, ν_{incoh} is seen to become increasingly non-negligible as d/λ increases resulting in slightly poorer agreement between the EC results and $\bar{\nu}$. This is compatible with the principle that the incoherent contribution to the intensity in the backward direction increases with ρd relative to the coherent contribution [15].

The agreement between the EC and the ν_{coh} results implies that the EC results as given in (39) represent the coherent field contribution to the RCS of the cloud. This claim may be supported by using (19) and (42) in (39) to obtain an expression that is proportional to N^2, a common characteristic of coherent intensities. In addition, as mentioned in Section II, the fact that the EC scattering is only in the $\pm\hat{\mathbf{x}}$ direction is compatible with coherent scattering of a wave normally incident on a slab of random scatterers [15, Ch. 14]. For the values of ρ and d/λ considered in Fig. 4, the EC results also provided good to excellent agreement with the average dipole results $\bar{\nu}$. For larger values of d/λ that will be considered below, the level of agreement between EC results and $\bar{\nu}$ would depend on the behavior of ν_{incoh} at these greater cloud thicknesses. Determination of this behavior, as well as other numerical calculations for these larger d/λ values, were not deemed computationally feasible.

2) Propagation Characteristics: As indicated in Section III, the reflection and transmission coefficients related to propagation through the half-wave dipole cloud are dependent on two parameters: s as defined in (19) and d/λ. Fig. 5 displays these coefficients as functions of d/λ for $\rho = 5/\lambda^3 (s = 0.116)$

based on the EC method. Also included in the figure are numerical results for attenuation through the dipole cloud obtained by adapting the forward scatter numerical results of Fig. 4(a). It is to be emphasized that the parameter d/λ does not relate to the distance of penetration within a cloud, but rather to the total thickness of the cloud. The individual plots in the figure will now be analyzed.

a) Cloud RCS: The plot which at $d/\lambda \to 0$ has a small value (i.e., a large negative value in dB) is the reflection coefficient $|B_0|^2$ of the cloud as given in (25). It is this result for small values of d/λ that was plotted in Fig. 4. Since the value of $|B_0|^2$ would be unity (i.e., 0 dB) if the cloud were a perfect conductor, any other value represents this reflection coefficient relative to a perfect conductor. The oscillatory behavior of this plot is due to interference between the waves reflected from the near and the far surfaces of the cloud. These oscillations, which have a period of $d/\lambda = 1/2$, attenuate with increasing cloud thickness as a result of the attenuation of the wave that reaches and is reflected back from the far surface. For large values of d/λ, the plot approaches a constant value which, from (25), is seen to be $|B_0|^2 \underset{\lim d/\lambda \to \infty}{\to} |D|^2$

$$D \equiv \frac{1-\beta}{1+\beta} \tag{43}$$

and which is the "asymptotic value" indicated in the figures. For small s, (C14) may be used to obtain

$$|B_0|^2 \underset{\lim d/\lambda \to \infty}{\to} \frac{s^2}{16}, s \ll 1 \tag{44}$$

$$R_{\text{asymp}} \underset{\lim d/\lambda \to \infty}{\to} 10 \log_{10} |B_0|^2 = 20 \log_{10} s - 12.04, s \ll 1. \tag{45}$$

This $|B_0|^2$ coefficient characterizes the energy returned by the cloud alone, and does not refer to its shielding characteristics. This analysis indicates, however, that for given dipole characteristics and spacing, there is a value of d/λ beyond which there is no increase in the cloud RCS.

b) Target RCS Attenuation: When region 2 is a perfectly conducting target, the reflection coefficient given by (28) is unity when $d/\lambda = 0$. This coefficient is therefore shown in the figures as the attenuation of target RCS due to the presence of the cloud. Its oscillations have the same period, and are attenuated in the same manner, as the reflection coefficient discussed above. Since this attenuation was attributed to the weakening of the wave as it passes through the cloud, the disappearance of the influence of the far surface would be the same for this case as for the case when region 2 consisted of free space. The reflection coefficient is therefore seen in the figures to approach the same asymptotic value as in the previous case, and taking the limit of (28) as $d/\lambda \to \infty$ produces results identical to (44) and (45) above. Care should be exercised in interpreting this result. Although from (28) $|B_0|^2 = 1$ when no cloud is present, the fact the cloud presence causes a reduction in its value indicates that it can be considered a measure of shielding effectiveness. The asymptotic value indicates that the RCS of the cloud has become large relative to the shielded RCS of the target. This can be particularly apparent when dealing with a pulsed wave rather than a continuous wave.

It is interesting to note from Fig. 5 that there is a value of d/λ at which the "shielding effectiveness" is greater than its asymptotic value. That is, the plot of target RCS attenuation under consideration is oscillatory within an envelope. The lower boundary of this envelope appears to be well below the asymptotic value of this attenuation.

Equation (28) can be rewritten as

$$B_0 = \frac{D - e^{-4\pi\beta_i(d/\lambda)} e^{-2jk_0\beta_r d}}{1 - De^{-4\pi\beta_i(d/\lambda)} e^{-2jk_0\beta_r d}} \quad \text{region 2 perfect conductor} \tag{46}$$

where D was defined in (43). Since $|D| < 1$ and for moderate values of d/λ the term $e^{-4\pi\beta_i(d/\lambda)}$ will also be small, the second term in the denominator may be ignored in relation to the first. Then

$$B_0 \approx D - e^{-4\pi\beta_i(d/\lambda)} e^{-2jk_0\beta_r d}, d/\lambda \ll 1/s. \tag{47}$$

When $s \ll 1, D \approx js/4$ so that, for small and moderate values of d/λ, the first term in (47) will be small relative to the second term so that

$$B_0 \approx -e^{-2\pi s(d/\lambda)} e^{-4\pi j(d/\lambda)(1+s^2/8)}, s \ll 1, d/\lambda \ll 1/s \tag{48}$$

from which

$$R = 10 \log_{10} |B_0|^2 \approx -c_0 s[2(d/\lambda)] \text{ dB}, \quad s \ll 1, \quad d/\lambda \ll 1/s \tag{49}$$

where $c_0 = 20\pi \log_{10} e \approx 27.2875$. The improvement in shielding effectiveness in this region is therefore $2c_0 s$ dB per d/λ.

c) Attenuation Through Cloud: The attenuation of the wave through the cloud is characterized by the transmission coefficient given in (26). The resulting transmitted power expressed in dB, and the numerical results for a corresponding dipole cloud, are seen to be virtually identical and to have a linear dependence on d/λ. For large values of this parameter, it is seen from (26) that

$$|A_2|^2 \underset{\lim d/\lambda \to \infty}{\to} \frac{16|\beta|^2}{|1+\beta|^4} e^{-4\pi\beta_i(d/\lambda)} \tag{50}$$

$$|A_2|^2 \underset{\lim d/\lambda \to \infty}{\to} \left(1 + \frac{s^2}{8}\right) e^{-2\pi s(d/\lambda)}, s \ll 1 \tag{51}$$

$$T = 10 \log_{10} |A_2|^2 \underset{\lim d/\lambda \to \infty}{\to} 20 \log_{10} \left(\frac{4|\beta|}{|1+\beta|^2}\right) - 2c_0\beta_i(d/\lambda) \text{ dB} \tag{52}$$

$$T \approx -c_0 s(d/\lambda) \text{dB}, s \ll 1. \tag{53}$$

Thus the rate of attenuation of the wave through the cloud is $c_0 s$ dB per d/λ. Using (19) and Fig. 3, this may be simplified to $T \approx -0.655(\rho\lambda^3)(d/\lambda)$ dB for a cloud of half wave dipoles.

It is seen that the rate of decrease of the transmission coefficient in (53) is half that given in (49) for the target RCS attenuation. This is obviously due to the fact that (53) represents only a "one-way" path while (49) represents a "two-way" path of the wave: towards the target, reflection from it, and back. That is, the rate of attenuation per distance is the same for the two cases, but the path in (49) is twice the path in (53).

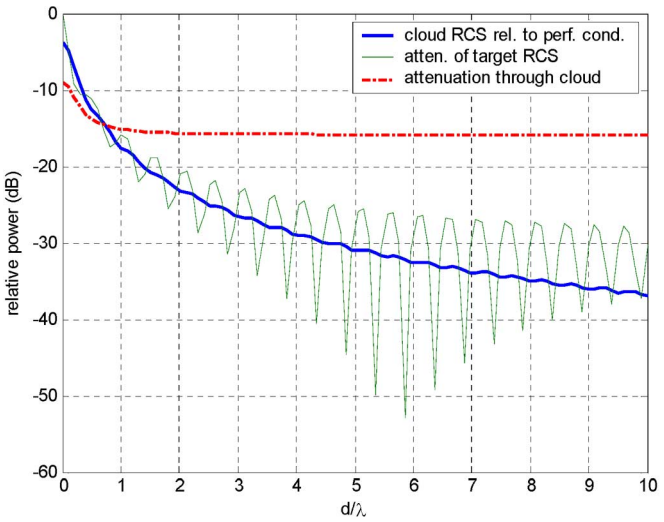

Fig. 6. Transmission and reflection coefficients for propagation through a dipole cloud when the number of dipoles per cross sectional area remains constant, $\rho(d/\lambda = 5) = 5/\lambda^3$.

As noted earlier, the EC results as characterized by (50) are indistinguishable in Fig. 5 from both the average and the coherent transmission intensity for the corresponding dipole cloud. The degree by which this excellent agreement continues for larger d/λ depends on the eventual behavior, currently unknown, of the incoherent contribution to this intensity.

3) Density Variation With Cloud Expansion: In the results presented thus far, variations of energy related parameters were considered as functions of cloud thickness d/λ, under the assumption of constant dipole density. However, in most situations, the cloud would consist of a given number of dipoles, and this cloud might change shape in response to aerodynamic influences. To simulate this, consider a cylindrical portion of the slab with axis normal to its planar boundaries, where A is its cross sectional area. This cylinder will contain

$$N = \rho A d \tag{54}$$

dipoles. It will be assumed that any change in d will result in a change in ρ such that N (and A) remain constant. Fig. 6 displays the reflection and transmission coefficients for the same range of d/λ as Fig. 5, but with the density ρ at the center of the range (i.e., $d/\lambda = 5$) having the same value, $5/\lambda^3$, as that used to obtain the results of Fig. 5. That is, at $d/\lambda = 5$ the results of Figs. 6 and 5 are identical.

Since the reference value of ρ was taken at $d/\lambda = 5$, its value is very large for small values of d/λ. As a result, the cloud RCS is very large when $d/\lambda \ll 1$ in Fig. 6 whereas in Fig. 5 it was very small. The attenuation T of the wave through the cloud is seen to reach an asymptotic value, whereas in Fig. 5 it decreased linearly (in dB). This indicates that T is dependent, in general, on the number of dipoles which are traversed by the wave, and not on the distance required to traverse them. This may be seen immediately from (53), with (19) and (54). It should be noted that when ρ is large in the vicinity of $d/\lambda \ll 1, s$ is not small so that (53) does hold in that region, thereby accounting for the variability of T when d/λ is small.

V. Conclusion

A method has been described to simulate a cloud of dipoles by an equivalent conducting continuum the conductivity of which depends on the dipole parameters and the average dipole density. Although this conductivity was derived for an infinitesimally narrow slab in which no inter-dipole coupling was present, it was found to provide useful RCS results for wide clouds as well. Since the RCS may be easily calculated for the conducting continuum, the coherent attenuation effects of the discrete dipole cloud may be found, and a closed form approximation for this attenuation may be derived.

Appendix

A. Uniform Current in Narrow Slab

Consider a uniform current density $\mathbf{J}$ flowing in a slab of thickness $d \ll \lambda$. The vector potential is

$$\mathbf{A}(\mathbf{r}) = \frac{\mu_0}{4\pi} \int_{\text{slab}} \mathbf{J}(\mathbf{r}') \frac{e^{-jkR}}{R} dV' \tag{A1}$$

where

$$\mathbf{J}(\mathbf{r}') = \begin{cases} J_0 \hat{\mathbf{z}}, & \mathbf{r}' \text{in slab} \\ 0, & \text{otherwise} \end{cases} \tag{A2}$$

$R = \sqrt{(x-x')^2 + (y-y')^2 + (z-z')^2}$ and the x-axis is normal to the slab. From symmetry it is clear that $\mathbf{A}(\mathbf{r})$ cannot be a function of y or z so that no generality is lost by assuming $y = z$ =0. In addition, since the slab is narrow, the value of x' will not change greatly in the integrand so that $x' = 0$ can be assumed. Therefore, $R = \sqrt{x^2 + y'^2 + z'^2} = \sqrt{x^2 + \rho'^2}$ and $dV' = dx' 2\pi\rho' d\rho'$, so that

$$\begin{aligned} \mathbf{A}(\mathbf{r}) &= \frac{\mu_0 J_0 x \hat{\mathbf{z}} d}{2} \int_0^\infty d\frac{\rho'}{x} \frac{\rho'}{x} \frac{e^{-jkx\sqrt{1+\left(\frac{\rho'}{x}\right)^2}}}{\sqrt{1+\left(\frac{\rho'}{x}\right)^2}} \\ &= \frac{\mu_0 J_0 x \hat{\mathbf{z}} d}{2} \int_1^\infty e^{-jkx\zeta} d\zeta = \frac{\mu_0 J_0 x \hat{\mathbf{z}} d}{2} \frac{e^{-jkx}}{jkx} \end{aligned} \tag{A3}$$

which employed the change of variables $\zeta = \sqrt{1 + (\rho'/x)^2}$ and the temporary assumption that k has an infinitesimal negative imaginary part [18]. Since $\nabla \cdot \mathbf{A} = 0$, the $\mathbf{E}$ and $\mathbf{H}$ fields may be obtained from $\mathbf{A}$ as

$$\mathbf{E} = -j\omega\mathbf{A} = -\frac{\eta_0 J_0 d e^{-jkx}}{2} \hat{\mathbf{z}}, \tag{A4}$$

$$\mathbf{H} = \frac{1}{\mu_0} \nabla \times \mathbf{A} = -\frac{\hat{\mathbf{y}}}{\mu_0} \frac{\partial A_z}{\partial x} = -\frac{J_0 d e^{-jkx}}{2} \hat{\mathbf{y}}. \tag{A5}$$

The time averaged Poynting vector is therefore

$$\mathbf{S}_{\text{avg}} = \frac{1}{2} \text{Re}(\mathbf{E} \times \mathbf{H}^*) = -\eta_0 |J_0|^2 \frac{d^2}{8} \hat{\mathbf{x}}. \tag{A6}$$

B. Uniform Current Density in Disk

Consider a uniform current density flowing in a disk shaped portion of a narrow slab. The axis of the disk is in the x-di-

rection, the disk has a thickness d, and a radius ρ_0. The vector potential is

$$\mathbf{A}(\mathbf{r}) = \frac{\mu_0}{4\pi} \int_{\text{disk}} \mathbf{J}(\mathbf{r}') \frac{e^{-jkR}}{R} dV' \tag{B1}$$

where

$$\mathbf{J}(\mathbf{r}') = \begin{cases} J_0\hat{\mathbf{z}}, & \mathbf{r}' \text{ in disk} \\ 0, & \text{otherwise} \end{cases} \tag{B2}$$

$$R = x\sqrt{1 + \frac{\rho^2}{x^2}\left[1 + \left(\frac{\rho'}{\rho}\right)^2 - 2\left(\frac{\rho'}{\rho}\right)\cos\phi'\right]}$$

$$\approx x\left\{1 + \frac{1}{2}\frac{\rho^2}{x^2}\left[1 + \left(\frac{\rho'}{\rho}\right)^2 - 2\left(\frac{\rho'}{\rho}\right)\cos\phi'\right]\right\} \tag{B3}$$

where $\rho' = \sqrt{y'^2 + z'^2}, \rho = \sqrt{y^2 + z^2}, \rho/|\mathrm{x}| \ll 1$ and $x' = 0$ was assumed. Therefore

$$\mathbf{A}(\mathbf{r}) \approx \frac{\mu_0 J_0 e^{-jkx} e^{-jk\frac{\rho}{2}\frac{\rho}{x}} d\hat{\mathbf{z}}}{4\pi x} \int_0^{\rho_0} \rho' d\rho' \times e^{-jk\frac{\rho}{2}\frac{\rho}{x}\left(\frac{\rho'}{\rho}\right)^2} \int_0^{2\pi} d\phi' e^{jk\rho\frac{\rho}{x}\left(\frac{\rho'}{\rho}\right)\cos\phi'}. \tag{B4}$$

The ϕ' integral can be evaluated as

$$\int_0^{2\pi} d\phi' e^{jk\rho\frac{\rho}{x}\left(\frac{\rho'}{\rho}\right)\cos\phi'} = 2\pi I_0\left(jk\rho\frac{\rho}{x}\left(\frac{\rho'}{\rho}\right)\right) = 2\pi J_0\left(k\rho\frac{\rho}{x}\left(\frac{\rho'}{\rho}\right)\right) \underset{\lim \frac{\rho}{x}\to 0}{=} 2\pi\left[1 - \left(k\rho\frac{\rho}{x}\frac{\rho'}{\rho}\right)^2\right] \tag{B5}$$

where $I_0(z)$ and $J_0(z)$ are Bessel Functions. Ignoring terms of higher order in ρ/x,

$$\mathbf{A}(\mathbf{r}) = \frac{\mu_0 J_0 d e^{-jkx} e^{-jk\frac{\rho}{2}\frac{\rho}{x}}\hat{\mathbf{z}}}{2x} \int_0^{\rho_0} \rho' d\rho' e^{-jk\frac{\rho}{2}\frac{\rho}{x}\left(\frac{\rho'}{\rho}\right)^2} = \frac{\mu_0 J_0 \rho^2 d e^{-jkx} e^{-jk\frac{\rho}{2}\frac{\rho}{x}}\hat{\mathbf{z}}}{4x}\left[\frac{e^{-jk\frac{\rho}{2}\frac{\rho}{x}\left(\frac{\rho_0}{\rho}\right)^2} - 1}{\left(-jk\frac{\rho}{2}\frac{\rho}{x}\right)}\right] = \frac{\mu_0 J_0 \rho_0^2 d e^{-jkx}\hat{\mathbf{z}}}{4x} + O\left(\frac{\rho}{x}\right)^2 \approx \frac{\mu_0 J_0 V e^{-jkx}\hat{\mathbf{z}}}{4\pi x}. \tag{B6}$$

Since $\nabla \cdot \mathbf{A} = 0$

$$\mathbf{E} = -j\omega\mathbf{A} = -\frac{jk^2 V}{4\pi x}\frac{J_0}{\omega\varepsilon_0} e^{-jkx}\hat{\mathbf{z}} \tag{B7}$$

$$\mathbf{H} = \frac{1}{\mu_0}\nabla \times \mathbf{A} = -\frac{\hat{\mathbf{y}}}{\mu_0}\frac{\partial A_z}{\partial x} = -\frac{jkJ_0 V e^{-jkx}}{4\pi x}\hat{\mathbf{y}} + O\left(\frac{1}{x^2}\right) \tag{B8}$$

$$\mathbf{S}_{\text{avg}} = \frac{1}{2}\text{Re}(\mathbf{E} \times \mathbf{H}^*) = -\frac{\hat{\mathbf{x}}}{2\eta_0}\left[\left(\frac{J_0}{\omega\varepsilon_0}\right)\left(\frac{Vk^2}{4\pi x}\right)\right]^2. \tag{B9}$$

C. Slab Properties

Assume the permittivity and permeability of the slab in region 1 are those of free space, but unlike free space the slab also has a conductivity σ. This is tantamount to an effective permittivity of the slab given by

$$\varepsilon_1 = \varepsilon_0(1 - js) \tag{C1}$$

where

$$s = \frac{\sigma}{\varepsilon_0\omega}. \tag{C2}$$

The wave vector in the slab then satisfies

$$k_1^2 = \omega^2\mu_0\varepsilon_0\sqrt{1+s^2}\frac{1-js}{\sqrt{1+s^2}} = k_0^2\sqrt{1+s^2}e^{j\theta}$$
$$\theta = \tan^{-1}(-s), -\frac{\pi}{2} < \theta < 0 \tag{C3}$$

where the branch is chosen to assure that $\text{Re}(k_1) > 0$ which leads to $\text{Im}(k_1) < 0$

$$k_1 = k_0(1+s^2)^{1/4}e^{j\theta/2}, \quad -\frac{\pi}{2} < \theta < 0. \tag{C4}$$

It is therefore possible to write

$$k = k_r - jk_i, k_i > 0. \tag{C5}$$

Now

$$\beta = \frac{\eta_0}{\eta_1} = \frac{k_1}{k_0} = \frac{k_r - jk_i}{k_0} = \beta_r - j\beta_i, \beta_r, \quad \beta_i > 0 \tag{C6}$$

and

$$\alpha = k_1 d = k_0 d\beta = 2\pi(d/\lambda)(\beta_r - j\beta_i) = \alpha_r - j\alpha_i, \alpha_r, \alpha_i > 0 \tag{C7}$$

where, from (C4),

$$\beta_r = (1+s^2)^{1/4}\cos(\theta/2) = \left(\frac{\sqrt{1+s^2}+1}{2}\right)^{1/2}$$
$$\beta_i = (1+s^2)^{1/4}\sin(|\theta|/2) = \left(\frac{\sqrt{1+s^2}-1}{2}\right)^{1/2}. \tag{C8}$$

This can also be used to obtain

$$\beta^2 = (1+s^2)^{1/2}e^{j\theta} \tag{C9}$$

so that

$$1 - \beta^2 = 1 - (1+s^2)^{1/2}\cos\theta - j(1+s^2)^{1/2}\sin\theta \tag{C10}$$

from which

$$|1-\beta^2|^2 = s^2, \quad |1+\beta^2|^2 = s^2 + 4. \tag{C11}$$

When s is small, from (C8)

$$\beta_r \approx 1 + \frac{s^2}{8}, \quad \beta_i \approx \frac{s}{2}, \quad s \ll 1. \tag{C12}$$

Then

$$|1-\beta| \approx \frac{s}{2}, \quad |1+\beta| \approx 2 + \frac{3s^2}{16},$$
$$|\beta| \approx 1 + \frac{s^2}{4}, \quad s \ll 1. \tag{C13}$$

It follows that

$$\frac{|1-\beta|}{|1+\beta|} \approx \frac{s}{4}, \quad s \ll 1. \tag{C14}$$

D. Random Media Scattering

For each realization m from among a total of M realizations, a vector component of the scattered field in a given direction may be divided into coherent and incoherent parts:

$$E_{\text{scat}}^{(m)} = E_{\text{coh}} + E_{\text{incoh}}^{(m)} \tag{D1}$$

where

$$E_{\text{coh}} = \frac{1}{M} \sum_{m=1}^{M} E_{\text{scat}}^{(m)} \tag{D2}$$

so that

$$\sum_{m=1}^{M} E_{\text{incoh}}^{(m)} = 0. \tag{D3}$$

From (D2), the coherent scattered field is not dependent on the particular realization. Recognizing from (40) and (D1) that, for a unit incident field

$$\nu^{(m)} = 4\pi E_{\text{scat}}^{(m)} E_{\text{scat}}^{(m)^*} = \nu_{\text{coh}} + 4\pi \left[E_{\text{coh}} E_{\text{incoh}}^{(m)^*} + E_{\text{incoh}}^{(m)} E_{\text{coh}}^{*} + |E_{\text{incoh}}^{(m)}|^2 \right] \tag{D4}$$

the average normalized RCS of the scattered wave over M realizations is

$$\bar{\nu} = \nu_{\text{coh}} + \nu_{\text{incoh}} \tag{D5}$$

where

$$\nu_{\text{coh}} = 4\pi |E_{\text{coh}}|^2, \quad \nu_{\text{incoh}} = \frac{4\pi}{M} \sum_{m=1}^{M} |E_{\text{incoher}}^{(m)}|^2 \tag{D6}$$

and (D3) was used.

ACKNOWLEDGMENT

The author gratefully acknowledges the stimulating discussions held with Dr. E. Tomer and with Mr. D. Lavan during the preparation of this work. The author also gratefully acknowledges useful suggestions proposed by Mr. A. Berkowitz and Mr. Z. Penner.

REFERENCES

[1] L. B. vanBrunt, *Applied ECM*. Dunn Loring, VA: EW Engineering, 1978, vol. 1.
[2] B. C. F. Butters, *Proc. Inst. Elect. Eng. Chaff*, vol. 129, no. 3, pt. F, pp. 197–201, June 1982.
[3] S. W. Marcus, "Dynamics and radar cross section density of chaff clouds," *IEEE Trans. Aerosp. Electron. Syst.*, vol. 40, no. 1, pp. 93–102, Jan. 2004.
[4] J. Paul, H. Anthony, B. Kochtubajda, and G. Kutznetsov, "Study of airflow in an Alberta hailstorm using chaff and polarization radar," in *Proc. 1997 28th Conf. Radar Meteorology*, Austin, TX, pp. 549–550.
[5] H. Jeske, "Modification of tropospheric propagation conditions," in *Conf. Proc. Ionosphere Modification and its Potential to Enhance or Degrade the Performance of Military Systems*, Bergen, Norway, May 28–31, 1990, (La Modification de l'Ionosphere et son Potentiel d'Amelioration ou de Degradation des Performances des Systemes Militaires), AD-A239 823, p33-1 thru p33-11.
[6] B. E. Martner, J. D. Marwitz, and R. A. Kropfli, "Radar observations of transport and diffusion in clouds and precipitation using TRACIR," *J. Atmos. Ocean. Technol.*, vol. 9, no. 3, pp. 226–241, Jun. 1992.
[7] S. V. Pakhomov, Z. T. Rapoport, and V. M. Sinel'nikov, "Investigations of the winter anomaly in ionospheric absorption in January 1981," *J. Atmos. Terr. Phys.*, vol. 46, no. 2, pp. 129–141, Feb. 1984.
[8] R. G. Wickliff and R. J. Garbacz, "The average backscattering cross section of clouds of randomized resonant dipoles," *IEEE Trans. Antennas Propag.*, vol. AP-22, no. 3, pp. 503–506, May 1974.
[9] P. Pouliguen, "Complete modeling of electromagnetic scattering by a cloud of dipoles," *Annales des Telecommunications*, vol. 48, no. 5–6, pp. 305–318, 1993.
[10] J. H. Van Vleck, F. Bloch, and M. Hamermesh, "Theory of radar reflections from wires or thin metallic strips," *J. Appl. Phys.*, vol. 18, pp. 274–294, 1947.
[11] O. Einarsson, "The wire," in *Electromagnetic and Acoustic Scattering of Simple Shapes*, J. J. Bowman, T. B. A. Senior, and P. L. E. Uslenghi, Eds. New York: Hemisphere, 1987, pp. 472–502.
[12] G. J. Burke and A. J. Poggio, Numerical electromagnetics code (NEC)—method of moments, UCTD-18834 Jan. 1981, Lawrence Livermore Laboratories.
[13] S. Kownacki, "Screening (shielding) effect of a chaff cloud," *IEEE Trans. Aerosp. Electron. Syst.*, Jul. 1967.
[14] E. C. Jordan and K. G. Balmain, *Electromagnetic Waves and Radiating Systems*. Englewood Cliffs, NJ: Prentice-Hall, 1968.
[15] A. Ishimaru, *Wave Propagation and Scattering in Random Media*. New York: Academic Press, 1978.
[16] E. F. Knott, J. F. Shaeffer, and M. T. Tuley, *Radar Cross Section*. Norwood, MA: Artech House, 1985.
[17] G. T. Ruck, D. E. Barrick, W. D. Stuart, and C. K. Krichbaum, *Radar Cross Section Handbook*. New York: Plenum Press, 1970.
[18] I. S. Gradshteyn and I. M. Ryzhik, *Tables of Integrals, Series, and Products*. New York: Academic Press, 1965.

Sherman W. Marcus (M'80–SM'89) received the B.A. and M.A. degrees in physics from Yeshiva University, in 1963 and 1965, respectively, and the Ph.D. degree in applied physics from the Catholic University of America, Washington, DC, in 1972.

As a Physicist for the U.S. Naval Ship Engineering Center, from 1967 to 1973, he was active in the investigation of nuclear weapons effects on ships. From 1973 to 1979, and from 1980 to the present, he has been on the research staff of RAFAEL, Haifa, where he currently holds the title of Research Fellow. From 1979 to 1980, he was a Research Engineer at IIT Research Institute in Annapolis, MD, where he continued to provide consulting services until 1990. From 1992 to 1998, he was also an Adjunct Senior Teaching Associate at the Technion, Israel Institute of Technology. During these periods, he was engaged in the development of analytical and numerical methods for predicting propagation and scattering of electromagnetic and acoustic waves, with emphasis on the effects of duct environments and on development and use of parallelization algorithms. His current area of interest is computer simulation of modern radars and electronic countermeasures. He has published many journal articles, and has presented papers and lectured at numerous professional conferences.